Published in "Journal of Materials Chemistry B 4(6): 1166–1174, 2016"
which should be cited to refer to this work.

http://doc.rero.ch

Synthesis, characterization, antibacterial activity and cytotoxicity of hollow TiO_2-coated CeO_2 nanocontainers encapsulating silver nanoparticles for controlled silver release†

J. Gagnon,*[ac] M. J. D. Clift,[b] D. Vanhecke,[b] I. E. Widnersson,[c] S.-L. Abram,[a] A. Petri-Fink,[b] R. A. Caruso,[c] B. Rothen-Rutishauser[b] and K. M. Fromm*[a]

Biomaterials as implants are being applied more extensively in medicine due to their on-going development and associated improvements, and the increase in human life expectancy. Nonetheless, biomaterial-related infections, as well as propagating bacterial resistance, remain significant issues. Therefore, there is a growing interest for silver-based drugs because of their efficient and broad-range antimicrobial activity and low toxicity to humans. Most newly-developed silver-based drugs have an extremely fast silver-ion release, increasing adverse biological impact to the surrounding tissue and achieving only short-term antimicrobial activity. Nanoencapsulation of these drugs is hypothesized as beneficial for controlling silver release, and thus is the aim of the present study. Initially, an amorphous or crystalline (anatase) titania (TiO_2) coating was synthesized around silver nanoparticle-containing (AgNP) ceria (CeO_2) nanocontainers using a sonication method forming AgNP/CeO_2/TiO_2 nanocontainers. These nanocontainers were characterized by high-resolution transmission electron microscopy, scanning electron microscopy, powder X-ray diffraction, gas sorption experiments and energy-dispersive X-ray spectroscopy. Silver release, monitored by using inductively coupled plasma optical emission spectroscopy, showed that these containers prevented silver release in water at neutral pH, and released the silver in concentrated nitric acid solution (pH = 1.1). The AgNP/CeO_2/TiO_2 nanocontainers showed an antibacterial activity against *E. coli*, however a concentration-dependent cytotoxicity towards a model epithelial barrier cell type (A549 cells) was observed. These nanocontainers offer the concept of potentially controlling silver delivery for the prevention of implant-associated infections.

1. Introduction

In the past decades, there has been a vast development and improvement in the use of biomedical implants.[1] However, the occurrence of bacterial infections remains a significant issue in the successful implantation of such materials.[2,3] For example, when a biofilm forms on the surface of an implant, *i.e.* when there is an irreversible attachment of microorganisms embedded in an extracellular matrix, the solution is normally to completely remove the implant and replace it with a new one. This results in unnecessary pain for the patient, elevated medical costs and a high risk of recidivism.[4–6] Due to the increasing resistance of bacteria to conventional antibiotics,[7] there are heightened demands for new approaches to impede the growth and onset of bacterial infections in order to prevent implant-related infections.

Silver-based drugs are an advantageous alternative to antibiotics as they have efficient antimicrobial activity towards a broad range of microorganisms (*e.g.* bacteria and fungi).[2] Additionally, in contrast to conventional antibiotics, silver resistance is not considered a clinical threat as silver has a multifaceted mode of action against bacteria.[8] Many silver drugs are already commercially available, such as silver nitrate solution for the prevention and cure of eye infections, and silver sulfadiazine in wound dressings for increasing wound repair and preventing wound infections, especially in burn wounds.[2] In addition to these salt-based silver medicinal applications, silver nanoparticles (AgNPs) have recently attracted increased interest in regards to the development of new antimicrobial (nano)materials, due to their high surface area and thus their heightened oxidative dissolution.[9–13]

The main issue with silver-based drugs is the rapid release of silver ions leading to high exposure concentrations that may

[a] *Department of Chemistry and Fribourg Center for Nanomaterials, University of Fribourg, Chemin du Musée 9, 1700 Fribourg, Switzerland. E-mail: katharina.fromm@unifr.ch, jacinthe.gagnon@iaf.inrs.ca*
[b] *Adolphe Merkle Institute, University of Fribourg, Chemin de Verdiers 4, 1700 Fribourg, Switzerland*
[c] *PFPC, School of Chemistry, The University of Melbourne, Melbourne, Victoria 3010, Australia*

† Electronic supplementary information (ESI) available

inflict adverse effects upon human cells, as demonstrated by many *in vitro* studies.[14–17] Moreover, prolonged exposure to high silver concentrations can lead to argyria,[18] a non-fatal condition giving a grayish-blue discoloration of the skin. For implants that remain within the human body for many years, it is therefore important to control the release of silver in order to avoid any undesired biological effects.

Recently, there has been a significant increase in the development of silver-containing coordination polymers, coatings and materials[19–27] that exhibit high levels of control over structure, stability and oxidative dissolution.[3] As an example, Dacarro *et al.*[28] demonstrated that self-assembled monolayers (SAM) of polyethylenimine are efficient for complexing silver cations and for anchoring AgNPs. These silver-containing SAM grafted on glass surfaces also exhibited antibacterial activity against *Escherichia coli* (*E. coli*) and *Staphylococcus aureus*.[28] Recently, Zhang *et al.*[29] developed biocompatible and degradable polyphosphoester-based nanoparticles that can release silver in a controllable manner over a 5 day period. This novel type of silver-containing nanoparticle carries silver as cations *via* the formation of silver acetylides and is promising for the treatment of lung infections.[29] Previously we have demonstrated that cerium oxide (ceria, CeO_2) nanocontainers can encapsulate AgNPs and possess the ability to control the release of silver *in vitro*.[30] These AgNP/CeO_2 containers allow for a slow and controlled silver release. After a period of three months in water, only 30% of the total amount of silver was released. However, non-triggered release of silver occurred continuously over the three-month period.

Further encapsulation of these materials, therefore, could prove advantageous in order to gain important control over the release of silver ions. Titanium(IV) dioxide (titania, TiO_2) is of significant interest for this purpose. Titania nano- and microparticles are, for instance, commonly used in sunscreens.[31] Furthermore, since metal-based implants, such as hip implants, are normally made of titanium or titanium alloys at the surface of which an oxide layer forms in contact with aqueous media,[32] titania is a material of choice for the advanced development of antimicrobial implant surfaces.

Therefore the aim of the present study was to develop and characterize silver-containing ceria-based nanocontainers coated with titania (AgNP/CeO_2/TiO_2 nanocontainers), to evaluate their antibacterial activity, and to further investigate their potential biocompatibility *in vitro*.

2. Materials and methods

2.1 Materials

All chemicals were purchased from Sigma-Aldrich (Switzerland) unless otherwise stated and were of the highest quality available. Polyvinylpyrrolidone (PVP) had an average molecular weight of 40 000 g mol^{-1}. Styrene and water were double-distillated prior to use. All other chemicals were used without any further purification.

The as-received non-ionic surfactant solution (Sigma, catalogue number QC1197) consisted of a mixture of different non-ionic surfactants. The ammonia-containing non-ionic surfactant solution was prepared by diluting the as-received solution (1 mL) in water (5 mL) and ammonium hydroxide 25% solution (2.8 mL).

Lysogeny broth (LB) culture medium for the antibacterial tests was provided by Sigma-Aldrich as ready-to-use. Agar plates were prepared by mixing agar (12 g), yeast (5 g), tryptone (10 g) and sodium chloride (5 g) in 1 L water. The solution was sterilized by autoclaving at a temperature of 121 °C and a pressure of 100 kPa for 20 min. The solution cooled to ~50 °C before being poured into sterile plastic Petri dishes. Subsequently, the agar plates were cooled to room temperature (RT) before being inverted and stored at 4 °C until required.

2.2 Synthesis of polystyrene (PS) nanospheres

PS nanospheres were prepared by emulsion polymerization using a method described by Kordas *et al.*[33] Briefly, the reaction mixture was prepared by mixing doubly-distillated styrene (3.70 g, 35.5 mmol), potassium persulfate ($K_2S_2O_8$ 0.30 g, 1.1 mmol), and sodium dodecyl sulfate ($CH_3(CH_2)_{11}SO_4Na$, 0.09 g, 0.3 mmol) in water (250 mL). The solution was stirred at 80 °C under argon for 42 h. The PS nanospheres were washed three times by centrifugation for 30 min at 10 000 rpm (11 648*g*). The supernatant was discarded and the NPs re-suspended in water.

2.3 Synthesis of AgNP/PS nanospheres

The synthesis of AgNPs was adapted from the procedure developed by Evanoff and Chumanov.[34] Initially, the AgNPs were synthesized by the reduction of silver(I) oxide by hydrogen in the presence of anionic PS nanospheres. The reaction mixture was prepared as follows: previously prepared PS nanospheres (0.140 g), silver(I) oxide (0.045 g, 0.2 mmol) and water (60 mL) were placed into a 250 mL flask and into an autoclave filled with 10 bar H_2 at 70 °C. After 4 h with constant stirring, the mixture was centrifuged for 30 min at 10 000 rpm (11 648*g*). The supernatant was discarded and the pellets were re-suspended in water (5 mL).

The method to encapsulate the AgNPs into the PS beads was adapted from Kumbhar and Chumanov.[35] Specifically, the AgNPs and PS mixture (2 mL) was mixed with acetone (5 mL). This mixture was sonicated at RT for 4 h followed by centrifugation for 30 min at 10 000 rpm (11 648*g*). The pellets were subsequently re-suspended in water (5 mL) and stored at RT.

2.4 Synthesis of CeO_2 and AgNP/CeO_2 nanocontainers

The sol–gel deposition method to synthesize the different nanocontainers was inspired by the work of Kartsonakis *et al.*[33] Cerium acetylacetonate ($Ce(acac)_3$, 0.7 g, 1.6 mmol), polyvinylpyrrolidone (0.3 g, 0.0075 mmol), urea (0.3 g, 5.0 mmol) and water (40 mL) were mixed for 5 min at RT. Then the template was added to the mixture: for forming the CeO_2 nanocontainers, PS nanospheres (0.30 g) were added, whereas for forming the AgNP/CeO_2 nanocontainers, AgNP/PS nanospheres (0.12 g) were added. The reaction proceeded at 100 °C for four to five days without any agitation. The suspension was centrifuged for 30 min at 15 000 rpm (26 208*g*). The supernatant was discarded and the pellets were re-suspended in water (40 mL). This washing step was repeated three times and the CeO_2-coated particles were dried in an oven at 40 °C for one day. Hollow CeO_2

http://doc.rero.ch

and AgNP/CeO_2 nanocontainers were subsequently obtained by removing the PS core by calcination in air in an oven at 600 °C for 4 h.

2.5 TiO_2 coating

In order to coat nanocontainers with titania, a ''core'' sol and a ''coating'' sol were prepared. In a typical synthesis, the ''core'' sol consisted of 30 mg of the nanocontainers to be coated and 480 μL of ammonia-containing non-ionic surfactant solution in 60 mL of ethanol. The ''coating'' sol consisted of 0.90 g (2.6 mmol) titanium butoxide dissolved in 60 mL of ethanol. Both sols were cooled in a fridge at 4 °C. To start the reaction, the sols were removed from the fridge, rapidly mixed together and placed in an ultrasonic bath at RT for 1 h. The nanocontainers coated with TiO_2 were aged overnight. The remaining unreacted titanium butoxide was removed by three successive centrifugation at 4000 rpm (1864*g*) and redispersion in ethanol steps. The nanocontainers were dried at RT in air overnight. The titania coating of these CeO_2/TiO_2 and AgNP/CeO_2/TiO_2 nanocontainers consisted at this stage of amorphous titania. In order to obtain anatase-based CeO_2/TiO_2 and AgNP/CeO_2/TiO_2 nanocontainers, the obtained materials underwent calcination in an oven at 500 °C for 2 h in air.

2.6 Characterization

Powder X-ray diffraction (PXRD) patterns of the samples were measured using a STOE Transmission X-Ray Powder Diffraction System. The nanocontainers were visualized by high-resolution transmission electron microscopy (HR-TEM) using a FEI Tecnai F20 microscope and by scanning electron microscopy (SEM) using a high-resolution field emission environmental SEM Quanta 200 FEI equipped with a dispersive X-ray spectroscopy (EDS) detector. Nitrogen sorption isotherms for the materials were measured at −196 °C using an Accelerated Surface Area and Porosimetry System ASAP 2010 or a Micromeritics Tristar 3000 system. The Brunauer–Emmett–Teller (BET) method[36] was used to calculate the specific surface areas and the Barrett–Joyner–Halenda (BJH) method[37] was used to determine the pore size distribution in the nanocontainers.

2.7 Silver release

Silver release experiments for AgNP/CeO_2/TiO_2 nanocontainers were performed using a method previously described.[30] In short, 5 duplicates of 75 mg of sample were deposited in the bottom of a well. The samples were covered with 1.2 mL of freshly distilled water and were incubated at RT in the dark. Over a 3 month period, aliquots of 500 μL were taken from the supernatant and were replaced by freshly distilled water. The aliquots were added to 3 mL of a 1% nitric acid solution and were stored in a well-sealed vial. After the 3 month period, the supernatant in each well was replaced by a 50% nitric acid solution and incubated for 4 h. Aliquots were taken and stored as before. The silver concentration in each vial was measured by inductively coupled plasma optical emission spectroscopy (ICP-OES) using a Perkin Elmer Optima 7000DV ICP-OES.

2.8 Antibacterial tests

The bactericidal activity of the nanocontainers was evaluated by determining the zone of growth inhibition using the agar diffusion method.[38,39] In order to facilitate the determination of the zone of growth inhibition, pellets were formed by pressing 90 mg of sample underneath 3 tonnes for 1 minute using a press.

The bacterial strain *E. coli* K-12 was used to perform the antibacterial tests. Prior to exposure, a single-cell colony was cultured and suspended in 1 mL of LB medium. Bacterial cultures were incubated overnight at 37 °C without agitation. Following the incubation period, 10 μL of the saturated bacterial solution was combined with 1 mL of fresh LB medium and incubated at 37 °C for an additional 2 h. Of the resulting broth, 100 μL was spread onto an agar plate until it was absorbed in the agar. The previously prepared pellet was placed in the centre of the agar plate and incubated in the inverted position overnight at 37 °C. The zone of growth inhibition was determined by measuring the distance between the pellet and the start of the bacterial growth.

2.9 Cell culture and exposure

Human adenocarcinoma alveolar type-II epithelial cells (A549 cell-line (ATCC, USA)), were cultured as previously described by Rothen-Rutishauser *et al.*[40] Exposures of the A549 cells to the different nanocontainer samples was performed in duplicates on three experiments in BD Falcon 2-chamber culture slides for four and seven days at concentrations of 58 and 174 mg per well (4.2 cm^2, 2 mL), as previously described by Gagnon *et al.*[30]

2.10 Epithelial cell cytotoxicity

Supernatants collected from the cell cultures following their exposure to the nanocontainer samples were assessed for levels of the cytosolic enzyme lactate dehydrogenase (LDH) as a measure of epithelial cell cytotoxicity, as previously described.[30] Results of all test samples were compared to the positive control, which consisted of 0.2% TritonX-100 in phosphate buffered saline (PBS). The negative control consisted of cells not exposed to nanocontainers. All analyses were repeated in triplicate (n = 3).

2.11 Epithelial cell morphology

Assessment of cellular morphology following exposure to the nanocontainer samples was conducted using confocal laser scanning microscopy (LSM), as previously described.[30,41] Briefly, fixed (3% paraformaldehyde in PBS) epithelial cell cultures were labelled with 1 : 50 dilution of phalloidin–rhodamine (F-actin cytoskeleton) and 1 : 100 dilution of 4′,6-diamidino-2-phenylindole (DAPI) (cell nuclei). Samples were mounted onto glass microscope slides using Glycergel (Dako, Carpinteria, USA) and imaged using an inverted LSM 710 Meta (Carl Zeiss, Jena, Germany) using a Plan-Apochromat 63×/1.4 lens (NA = 1.3) with 0.3 μm z-stacks to enable spatial investigation in 3D.

2.12 Statistical and data analysis

Silver release experiments were performed as quadruplicates (n = 4), whereas antibacterial and cytotoxicity tests were performed

http://doc.rero.ch

in triplicate ($n = 3$) in three experiments. Silver release, antibacterial and cytotoxicity results are presented as the mean ± standard error of the mean. Cytotoxicity data sets are normally distributed (not shown), enabling a parametric two-way ANOVA to be conducted with subsequent Tukey's *post hoc* test (SPSS, IBM, USA). Data sets were considered as significant when $p < 0.05$.

3. Results and discussion

3.1 Synthesis

The AgNP/CeO_2/TiO_2 nanocontainers were synthesized *via* a template-assisted method as illustrated in Fig. 1. The synthesis of the AgNP/CeO_2 nanocontainers was performed as previously described.[30] The PS core was removed by calcination, which also ensured that organic residues from the synthesis were removed. Afterwards, the AgNP/CeO_2 nanocontainers were further coated with titania *via* the hydrolysis and condensation of titanium(IV) butoxide under sonication.[42]

The use of a mixture of non-ionic surfactants has been previously demonstrated to be successful for coating a variety of particles with TiO_2.[43] Alternatively, single nonionic surfactants could be used, however the effects of using single surfactants for this application have not yet been explored. We demonstrate here that the addition of the ammonia-containing non-ionic surfactant solution was necessary to control the titania coating thickness and the sonication time needs to be kept to its minimum in order to prevent disintegration of the CeO_2 shell structure (see ESI†). In order to study the TiO_2 coating morphology and to compare results with AgNP/CeO_2/TiO_2 nanocontainers, CeO_2 nanocontainers were also coated with TiO_2, resulting in the CeO_2/TiO_2 nanocontainers.

After the TiO_2 coating step (Section 2.5), the titania shell on the CeO_2/TiO_2 nanocontainers was clearly visible *via* TEM (Fig. 2A), as TiO_2 is less electron dense compared to CeO_2. The atomic planes of CeO_2 can be observed using HR-TEM (Fig. 2B inset). The lattice spacing of 0.30 nm corresponds to the [1 1 1] lattice plane of CeO_2.[44–46]

The PXRD patterns of the CeO_2/TiO_2 and AgNP/CeO_2/TiO_2 nanocontainers show the presence of CeO_2 (Fig. 3). In addition, metallic silver is observed in the PXRD pattern of the AgNP/CeO_2/TiO_2 nanocontainers before calcination due to the presence of silver nanoparticles. However, TiO_2 is not detected by PXRD at this stage as it is amorphous. Nonetheless, the presence of titanium along with cerium and silver contents could be detected in EDS (Fig. S3, ESI†). It is possible to transform the TiO_2 coating into the anatase phase *via* calcination at 500 °C (Fig. 4). The double-shell structure of the CeO_2/TiO_2 nanocontainers can still be observed in TEM images (Fig. 5). The crystalline nature of the TiO_2 layer can be observed using HR-TEM (Fig. 5B-inset) and the crystal lattice spacing of 0.35 nm in the outer layer corresponds to the typical spacing for anatase [1 0 1] lattice plane.[47–49]

By comparing the TEM images of the CeO_2/TiO_2 nanocontainers before (Fig. 2) and after calcination (Fig. 5), there is an indication of increased porosity within the coating, which was confirmed by gas sorption experiments. Before coating with TiO_2, the CeO_2 nanocontainers have a Brunauer–Emmett–Teller (BET) surface area of 110 $m^2\ g^{-1}$ and pore sizes of 6–10 nm. After coating with amorphous TiO_2, the BET surface area increased to 168 $m^2\ g^{-1}$,

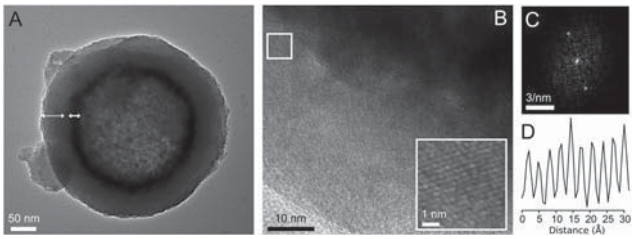

Fig. 2 CeO_2/TiO_2 nanocontainers before calcination. TEM (A), HR-TEM (B), fast Fourier transform (FFT) images (C) and FFT calibrated profile plot (D) of the selected area (B-inset). The CeO_2 shell (inner) and TiO_2 coating (outer) are indicated by solid and dashed arrows, respectively.

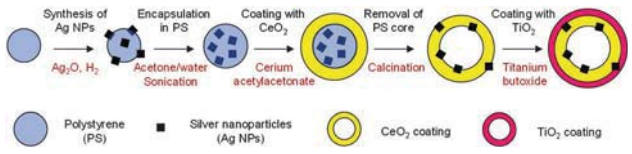

Fig. 1 Synthesis of AgNP/CeO_2/TiO_2 nanocontainers. PS beads (diameters of 220 ± 15 nm) that serve as templates were first synthesized *via* an emulsion polymerization method. AgNPs (40 ± 9 nm) were synthesized on the surface of the PS beads by reducing silver oxide (Ag_2O) in an autoclave under hydrogen pressure. AgNPs could then be encapsulated into the PS beads *via* the sonication of the AgNP/PS beads in a water/acetone mixture. This template was then coated with ceria *via* sol–gel deposition. Calcination of the resulting AgNP/PS/CeO_2 particles was demonstrated to be a fast and efficient way to remove the PS core, resulting in AgNP/CeO_2 nanocontainers.[30] These nanocontainers were coated with titania *via* a sonication method using titanium butoxide as the precursor.

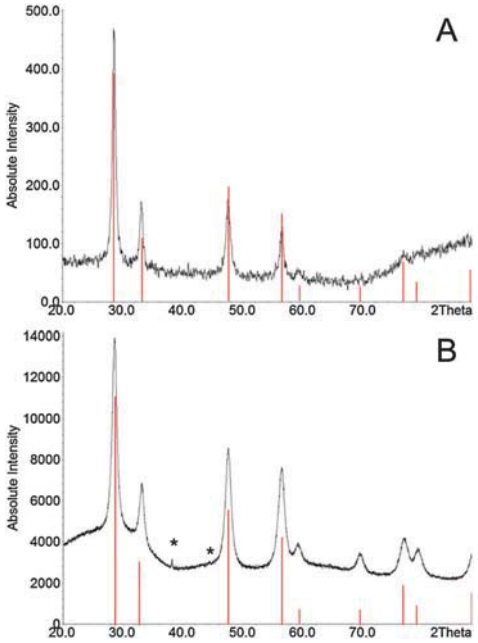

Fig. 3 PXRD patterns of CeO_2/TiO_2 nanocontainers (A) and AgNP/CeO_2/TiO_2 nanocontainers (B) before calcination. The red lines and stars indicate the theoretical positions for CeO_2 (JCPS no. 34-0394) and elemental silver (JCPS no. 04-0783) XRD peaks, respectively.

http://doc.rero.ch

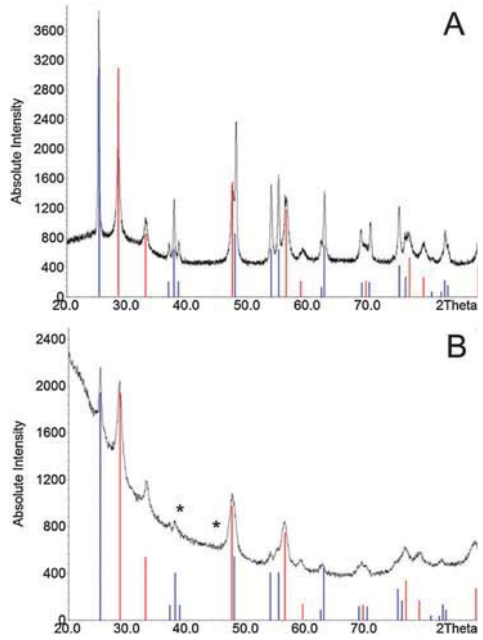

Fig. 4 PXRD patterns of CeO_2/TiO_2 nanocontainers (A) and AgNP/CeO_2/TiO_2 nanocontainers (B) after calcination. The red lines, blue lines and stars indicate the theoretical positions for CeO_2 (JCPS no. 34-0394), anatase (JCPS no. 21-1272) and elemental silver (JCPS no. 04-0783) peaks, respectively.

while the pore sizes were reduced to 2–5 nm. These findings indicate a decreased porosity of the nanocontainers following amorphous titania coating. After calcination, the BET surface area decreased to 68 $m^2\ g^{-1}$ and the pore sizes increased to between 6–8 nm, demonstrating the increase in pore size of the CeO_2/TiO_2 nanocontainers after calcination, which is consistent with the TEM observations (compare Fig. 2 and 5). Since egress from within a nanocontainer is decreased for reduced pore sizes,[50] nanocontainers coated with amorphous TiO_2 are preferred for controlling the silver release and therefore were used for further testing of the AgNP/CeO_2/TiO_2 nanocontainers.

SEM showed the morphology of the AgNP/CeO_2/TiO_2 nanocontainers not to be completely spherical (Fig. 6A). This is mainly due to an uneven TiO_2 coating around the CeO_2 shell (Fig. 6B), to the frequent encapsulation of more than one nanocontainer within the same TiO_2 coating (Fig. 6C) and some secondary nucleation TiO_2 particles. This is commonly observed in coating particles with titania.[43]

In order to evaluate how effectively the newly-developed AgNP/CeO_2/TiO_2 nanocontainers retained their silver content, silver release experiments were performed. The silver release was expected to be slower with these new nanocontainers compared to the AgNP/CeO_2 nanocontainers due to the additional TiO_2 coating that further hinders the silver from diffusing out of the nanocontainer. Fig. 7A presents the silver release for the first 10 days after immersion in water. There was an initial burst of silver release during the first day after immersion and then the cumulative silver concentration reached a plateau, indicating that no further silver release was detected by the ICP-OES. In addition, the total silver release remained below 5 ppm for a 75 mg sample in 1 mL of water. This concentration is lower than the half maximal inhibitory concentration (IC_{50}) reported for some mammalian cells, such as L929 murine fibroblasts (IC_{50}: 15–21 ppm using silver nitrate).[51] On the other hand, this value is higher than the minimum inhibitory concentration (MIC) of silver ions ($AgNO_3$)

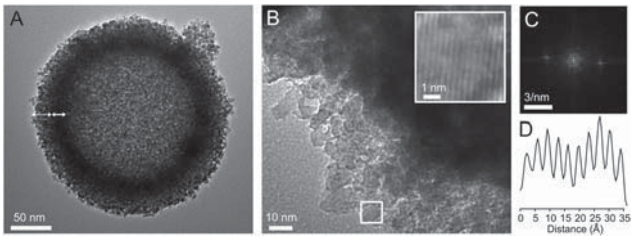

Fig. 5 CeO_2/TiO_2 nanocontainers after calcination. TEM (A), HR-TEM (B), FFT images (C) and FFT calibrated profile plot (D) of the selected area (B-inset). The CeO_2 shell (inner) and TiO_2 coating (outer) are indicated by the solid and dashed arrows, respectively.

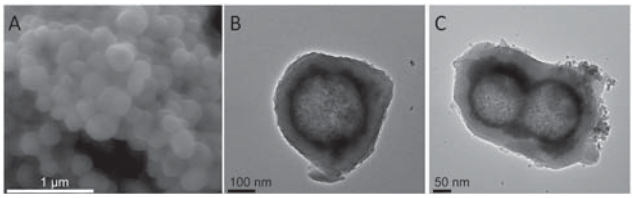

Fig. 6 SEM (A) and TEM (B and C) images of the AgNP/CeO_2/TiO_2 nanocontainers.

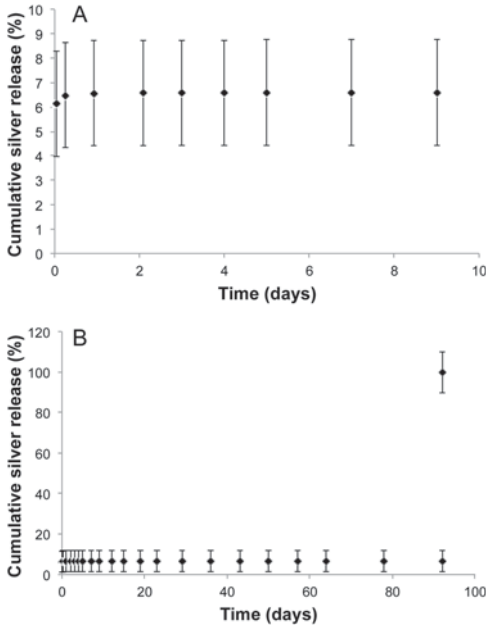

Fig. 7 Total silver release in percentage from AgNP/CeO_2/TiO_2 nanocontainers for the first 9 days (A) and over 92 days (B). At day 92, the silver concentration was measured before and after the addition of nitric acid. The experiments were performed in 5 duplicates (n = 5). Note that the error bars appear large in image A due to the low scale of the y-axis.

http://doc.rero.ch

against *E. coli*, which has been reported to be 3 μM (3.23 ppm).[2,52] This material is therefore promising since the quantity of silver release lies within this therapeutic window for antibacterial activity against *E. coli* while it is expected to have little impact on mammalian cells.

The rapid silver release can be considered as small NPs tend to undergo oxidative dissolution faster than larger NPs. As described by Borm *et al.*,[53] particles with a smaller radius of positive curvature (convex) tend to be energetically unstable, thus have a higher tendency to oxidize and be released as Ag^+. In addition, different nanoparticle shapes of the same material can influence the dissolution rate,[53,54] so that the AgNP shapes may also influence the silver release. The formation of an insoluble silver oxide (Ag_2O) layer on the surface of the AgNPs may also slow down the release of Ag^+ over time, similar to what was observed by Pallavicini *et al.*[55]

Some AgNPs can infrequently be observed during TEM analysis on the surface of the AgNP/CeO_2/TiO_2 nanocontainers (Fig. 8). These are attributed to a small amount of silver that dissolved into ethanol during the TiO_2 layer synthesis and reduced back into NPs on the surface of TiO_2 shell. Because these new AgNPs are directly exposed to the solution, they might have partly contributed to the initial silver release burst.

Over 3 months no further silver release was detected (Fig. 7B). In order to ensure that the nanocontainers still contain silver at the end of the silver release study and to check if the silver release could be triggered, the supernatant was replaced by concentrated nitric acid and was incubated for a few hours. This ensured that all the remaining silver nanoparticles were oxidized to Ag^+. The silver concentration in this final solution was ~42 ppm (100%), which is significantly higher than the cumulative silver release in water after 3 months, as shown in Fig. 7B.

The silver release experiments thus clearly demonstrate that the AgNP/CeO_2/TiO_2 nanocontainers are efficient in encapsulating AgNPs. In fact, even after a period of 3 months, only ~7% of the total silver load was released, with the release of the remaining silver being triggered *via* the oxidation of silver using nitric acid. This latter property is interesting as the purpose of this research was to develop antimicrobial coatings for the prevention of implant infections caused by bacteria. The bacterial metabolism leads to a decrease of the pH in their environment,[56–60] which could promote the oxidation of silver and increase the silver ion release from the above nanocontainers. The silver release experiments in other media (in phosphate buffered saline and in mild acidic conditions) are currently in progress.

Similar to various other silver-releasing surfaces that have been recently developed,[3] the initial release could protect implants against infections during the critical period, *i.e.* the post-surgery period during which a biomaterial is particularly vulnerable to microbial invasion.[3,61] The AgNP/CeO_2/TiO_2 nanocontainers have the additional advantage of retaining silver for prolonged periods (>3 months). This silver is therefore available for infections that can occur a long time after surgery. Another advantage of retaining silver over long periods of time is to improve the biocompatibility of silver-containing materials by avoiding the unspecific release of silver and thus prevents the undesired side effects of silver in absence of infections. These nanocontainers are therefore highly promising for drug delivery systems. In this regard, to make sure that they will be efficient for killing bacteria and that they are biocompatible, antibacterial activity against *E. coli* as well as the impact these nanocontainers have upon mammalian cells, specifically human A549 epithelial cells, were assessed.

3.2 Antibacterial activity

The bactericidal activity of CeO_2/TiO_2 nanocontainers and AgNP/CeO_2/TiO_2 nanocontainers was evaluated by the disc diffusion method.[38,39] The CeO_2/TiO_2 nanocontainers did not demonstrate any antibacterial activity (Fig. 9A). This is consistent with other studies that demonstrated little or no antimicrobial activity for CeO_2 or TiO_2 materials.[62–66] On the other hand, the AgNP/CeO_2/TiO_2 nanocontainers demonstrated a zone of growth inhibition of 0.5 mm around the pellet (Fig. 9B and C). This value is smaller than the zone of growth inhibition (2.0 mm) observed for AgNP/CeO_2 nanocontainers,[30] but it is consistent with the silver release, which is the antimicrobial agent. Since the AgNP/CeO_2/TiO_2 nanocontainers release less silver in normal conditions than those without the TiO_2 coating, they are expected to have a smaller zone of growth inhibition. This test nonetheless demonstrates the antibacterial activity of the silver in this material. These findings highlight that the TiO_2 layer hinders the silver release from the nanocontainers.

3.3 Epithelial cell viability and morphology

The human adenocarcinomic alveolar epithelial type II cell line A549 was chosen for the cytotoxicity tests as it is an excellent

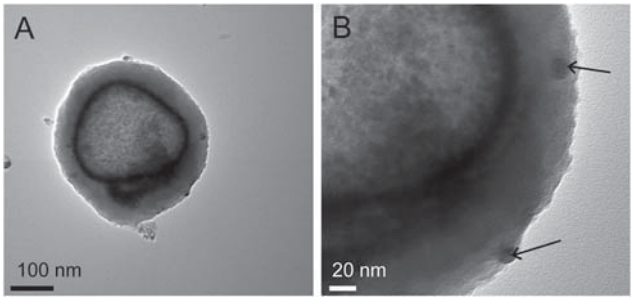

Fig. 8 TEM images of AgNP/CeO_2/TiO_2 nanocontainers before calcination demonstrating the presence of AgNPs on the surface of the TiO_2 shell, as indicated by the arrows.

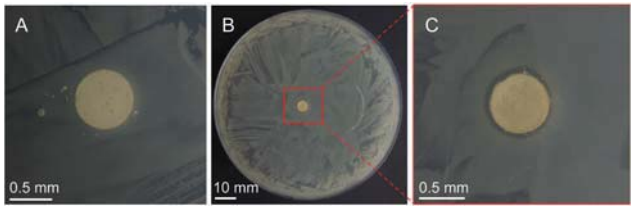

Fig. 9 Photographs of disc diffusion tests of CeO_2/TiO_2 nanocontainers (A) and AgNP/CeO_2/TiO_2 nanocontainers (B and C).

http://doc.rero.ch

model for barrier cell types, commonly used in many toxicity studies[67–69] and therefore allows for a good comparison between (nano)materials.

A significant decrease ($p < 0.05$) in LDH release from A549 cells was observed following exposure to 174 mg per well (87 mg mL^{-1}, 41.4 mg cm^{-2}) compared to the negative control after both 4 and 7 days (Fig. 10A). This effect can be attributed to an immediate onset of cell death, most likely necrosis, induced by the AgNP/CeO_2/TiO_2 nanocontainers. This effect has previously been observed for nanocontainers with a greater silver release, which also caused immediate necrosis,[30] and is further supported by the non-specific F-actin cytoskeleton (phalloidin) staining throughout the sample as observed *via* LSM (Fig. 10C) compared to the negative control (Fig. 10B). In addition the LDH assay demonstrated a reduced cytotoxicity for cells exposed to the lower concentration of AgNP/CeO_2/TiO_2 nanocontainers (58 mg per well, 29 mg mL^{-1}, 13.8 mg cm^{-2}) (Fig. 10A), specifically after 7 days, although increased cytotoxicity towards the model epithelial barrier cell type (A549 cells) compared to AgNP/CeO_2 nanocontainers.[30] This was further supported by LSM analysis that showed that at this concentration the A549 cells exhibited early morphological signs of cell death (data not shown).

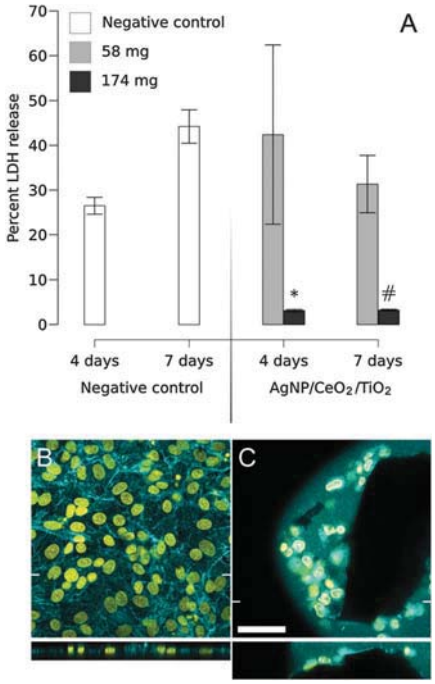

Fig. 10 Cytotoxicity to A549 epithelial cells as determined by LDH assay (A) of 58 mg per well (grey) and 174 mg per well (black) of AgNP/CeO_2/TiO_2 nanocontainers after 4 and 7 days of exposure. Data is represented as the percent mean ± standard error of the mean compared to the positive control (0.2% TritonX-100). * and # represent $p < 0.05$ compared to the negative control at 4 and 7 days respectively. The LSM images show the *XY* panel and below it the *XZ* panel of the negative control (B) and the AgNP/CeO_2/TiO_2 nanocontainers (C). The negative control corresponds to cell culture medium only. Cell nuclei and F-actin are stained with DAPI (yellow) and rhodamine–phalloidin (cyan) respectively. The scale bar corresponds to 50 μm.

4. Conclusions

Ceria-based nanocontainers were coated with TiO_2 in a very efficient and reproducible manner. This yielded both CeO_2/TiO_2 and AgNP/CeO_2/TiO_2 nanocontainers. In the case of AgNP/CeO_2/TiO_2 nanocontainers, the AgNPs were mainly encapsulated within the CeO_2 shell inside the TiO_2 layer and only a small amount were present on the outer surface of the TiO_2 layer. These nanocontainers demonstrated exceptional control over the silver release with only 7% of the silver content released when immersed in water over a 3 month period, and the release of the remaining silver able to be triggered on the addition of nitric acid. The AgNP/CeO_2/TiO_2 nanocontainers demonstrated an increased antibacterial activity against *E. coli*, although increased cytotoxicity towards a model epithelial barrier cell type (A549 cells) compared to AgNP/CeO_2 nanocontainers. Despite improvements needed regarding their mammalian cell biocompatibility, these nanocontainers have some potential for possible application in the controllable delivery of silver for preventing implant-related infections.

Acknowledgements

The authors are grateful for the financial support from the Swiss National Science Foundation (NRP-62 and Doc.Mobility Fellowship), the University of Fribourg, the Fribourg Center for Nanomaterials (FriMat), the Adolphe Merkle Foundation and The University of Melbourne. They are also grateful to Anne Schuwey for her help with the synthesis, Yuki Umehara for her help with cell culture and the Melbourne Advanced Microscopy Facility, Australia, for use of the electron microscopy facilities.

Notes and references

1 C. Eingartner, *Ortop. Traumatol. Rehabil.*, 2007, **9**, 8–14.
2 S. Eckhardt, P. S. Brunetto, J. Gagnon, M. Priebe, B. Giese and K. M. Fromm, *Chem. Rev.*, 2013, **113**, 4708–4754.
3 P. Pallavicini, G. Dacarro, Y. A. Diaz-Fernandez and A. Taglietti, *Coord. Chem. Rev.*, 2014, **275**, 37–53.
4 R. O. Darouiche, *N. Engl. J. Med.*, 2004, **350**, 1422–1429.
5 K. H. Mayer and S. C. Schoenbaum, *Prog. Cardiovasc. Dis.*, 1982, **25**, 43–54.
6 J. W. Costerton, P. S. Stewart and E. P. Greenberg, *Science*, 1999, **284**, 1318–1322.
7 M. Bell, *JAMA Intern. Med.*, 2014, **174**, 1920–1921.
8 I. Chopra, *J. Antimicrob. Chemother.*, 2007, **59**, 587–590.
9 M. J. Hajipour, K. M. Fromm, A. A. Ashkarran, D. Jimenez de Aberasturi, I. R. de Larramendi, T. Rojo, V. Serpooshan, W. J. Parak and M. Mahmoudi, *Trends Biotechnol.*, 2013, **30**, 499–511.
10 C. Baker, A. Pradhan, L. Pakstis, D. J. Pochan and S. I. Shah, *J. Nanosci. Nanotechnol.*, 2005, **5**, 244–249.
11 A. Panáček, L. Kvítek, R. Prucek, M. Kolář, R. Večeřová, N. Pizúrová, V. K. Sharma, T. Navěčná and R. Zbořil, *J. Phys. Chem.*, 2006, **110**, 16248–16253.

http://doc.rero.ch

http://doc.rero.ch

12 K. N. Thakkar, S. S. Mhatre and R. Y. Parikh, *Nanomedicine*, 2010, **6**, 257–262.
13 E. T. Hwang, J. H. Lee, Y. J. Chae, Y. S. Kim, B. C. Kim, B.-I. Sang and M. B. Gu, *Small*, 2008, **4**, 746–750.
14 J. M. Schierholz, L. J. Lucas, A. Rump and G. Pulverer, *J. Hosp. Infect.*, 1998, **40**, 257–262.
15 N. R. Panyala, E. M. Pena-Méndez and J. Havel, *J. Appl. Biomed.*, 2008, **6**, 117–129.
16 E. Sudmann, H. Vik, M. Rait, K. Todnem, K.-J. Andersen, K. Julsham, O. Flesland and J. Rungby, *Med. Prog. Technol.*, 1994, **20**, 179–184.
17 H. Vik, K. J. Andersen, J. Julshamn and K. Todnem, *Lancet*, 1985, **325**, 872.
18 T. D. Luckey and B. Venugopal, *Metal toxicity in mammals: Chemical toxicity of metals and metalloids*, Plenum Press, New York, NY, 1978.
19 A. Y. Robin, M. Meuwly, K. M. Fromm, H. Goesmann and G. Bernardinelli, *CrystEngComm*, 2004, **6**, 336–343.
20 A. Y. Robin, J. L. Sague Doimeadios and K. M. Fromm, *CrystEngComm*, 2006, **8**, 403–416.
21 A. Y. Robin, J. L. Sague Doimeadios, A. Neels, T. V. Slenters and K. M. Fromm, *Inorg. Chim. Acta*, 2007, **360**, 212–220.
22 T. V. Slenters, J. L. Sague Doimeadios, P. S. Brunetto, S. Zuber, A. Fleury, L. Mirolo, A. Y. Robin, M. Meuwly, O. Gordon, R. Landmann, A. U. Daniels and K. M. Fromm, *Materials*, 2010, **3**, 3407–3429.
23 T. V. Slenters, I. Hauser-Gerspach, A. U. Daniels and K. M. Fromm, *J. Mater. Chem.*, 2008, **18**, 5359–5362.
24 J. L. Sague Doimeadios and K. M. Fromm, *Cryst. Growth Des.*, 2006, **6**, 1566–1568.
25 K. M. Fromm, E. D. Gueneau, A. Y. Robin, W. Maudez, J. L. Sague Doimeadios and R. Bergougnant, *Z. Anorg. Allg. Chem.*, 2005, **631**, 1725–1740.
26 M. Varisco, N. Khanna, P. S. Brunetto and K. M. Fromm, *ChemMedChem*, 2014, **9**, 1221–1230.
27 M. Priebe and K. M. Fromm, *Part. Part. Syst. Charact.*, 2014, **31**, 645–651.
28 G. Dacarro, L. Cucca, P. Grisoli, P. Pallavicini, M. Patrini and A. Taglietti, *Dalton Trans.*, 2012, **41**, 2456–2463.
29 F. Zhang, J. A. Smolen, S. Zhang, R. Li, P. N. Shah, S. Cho, H. Wang, J. E. Raymond, C. L. Cannon and K. L. Wooley, *Nanoscale*, 2015, **7**, 2265–2270.
30 J. Gagnon, M. J. D. Clift, D. Vanhecke, D. A. Kuhn, P. Weber, A. Petri-Fink, B. Rothen-Rutishauser and K. M. Fromm, *J. Mater. Chem. B*, 2015, **3**, 1760–1768.
31 T. G. Smijs and S. Pavel, *Nanotechnol., Sci. Appl.*, 2011, **4**, 95–112.
32 E. A. B. Effah, P. D. Bianco and P. Ducheyne, *J. Biomed. Mater. Res.*, 1995, **29**, 73–80.
33 I. Kartsonakis, I. Daniilidis and G. Kordas, *J. Sol-Gel Sci. Technol.*, 2008, **48**, 24–31.
34 D. D. Evanoff and G. Chumanov, *J. Phys. Chem. B*, 2004, **108**, 13948–13956.
35 A. S. Kumbhar and G. Chumanov, *Chem. Mater.*, 2009, **21**, 2835–2839.
36 S. Brunauer, P. H. Emmett and E. Teller, *J. Am. Chem. Soc.*, 1938, **60**, 309–319.
37 E. P. Barrett, L. G. Joyner and P. P. Halenda, *J. Am. Chem. Soc.*, 1951, **73**, 373–380.
38 K. E. Cooper, *Nature*, 1955, **176**, 510–511.
39 B. Bonev, J. Hooper and J. Parisot, *J. Antimicrob. Chemother.*, 2008, **61**, 1295–1301.
40 B. M. Rothen-Rutishauser, S. G. Kiama and P. Gehr, *Am. J. Respir. Cell Mol. Biol.*, 2005, **32**, 281–289.
41 A. Lehmann, C. H. Brandenberger, F. Blank, P. Gehr and B. Rothen-Rutishauser, A 3D Model of the Human Epithelial Airway Barrier, in *Alternative Technologies to Animal Testing*, ed. M. L. Yarmush and R. S. Langer, Artech House, 2010, pp. 239–260.
42 H. Li, S. G. Sunol and A. K. Sunol, *Nanotechnology*, 2012, **23**, 294012.
43 A. F. Demirörs, A. van Blaaderen and A. Imhof, *Langmuir*, 2010, **26**, 9297–9303.
44 F. Zhang, S.-W. Chan, J. E. Spanier, E. Apak, Q. Jin, R. D. Robinson and I. P. Herman, *Appl. Phys. Lett.*, 2002, **80**, 127–129.
45 L. Wu, H. J. Wiesmann, A. R. Moodenbaugh, R. F. Klie, Y. Zhu, D. O. Welch and M. Suenaga, *Phys. Rev. B: Condens. Matter Mater. Phys.*, 2004, **69**, 125415.
46 R. C. Deusa, M. Cilensec, C. R. Foschinic, M. A. Ramireza, E. Longoc and A. Z. Simõesa, *J. Alloys Compd.*, 2013, **550**, 245–251.
47 L. Miao, S. Tanemura, Y. Kondo, M. Iwata, S. Toh and K. Kaneko, *Appl. Surf. Sci.*, 2004, **238**, 125–131.
48 I. Djerdj, A. M. Tonejc, M. Bijelić, V. Vranesa and A. Turković, *Vacuum*, 2005, **2005**, 371–378.
49 B. Liu, L.-M. Liu, X.-F. Lang, H.-Y. Wang, X. W. D. Lou and E. S. Aydil, *Energy Environ. Sci.*, 2014, **7**, 2592–2597.
50 Y. Levin, M. A. Idiart and J. J. Arenzon, *Physica A*, 2005, **354**, 95–100.
51 G. Müller and A. Kramer, *J. Antimicrob. Chemother.*, 2008, **61**, 1281–1287.
52 C.-N. Lok, C.-M. Ho, R. Chen, Q.-Y. He, W.-Y. Yu, H. Sun, P. K.-H. Tam, J.-F. Chiu and C.-M. Che, *JBIC, J. Biol. Inorg. Chem.*, 2007, **12**, 527–534.
53 P. Borm, F. C. Klaessig, T. D. Landry, B. Moudgil, J. Pauluhn, K. Thomas, R. Trottier and S. Wood, *Toxicol. Sci.*, 2006, **90**, 23–32.
54 R. Tang, C. A. Orme and G. H. Nancollas, *ChemPhysChem*, 2004, **5**, 688–696.
55 P. Pallavicini, A. Taglietti, G. Dacarro, Y. A. Diaz-Fernandez, M. Galli, P. Grisoli, M. Patrini, G. S. De Magistris and R. Zanoni, *J. Colloid Interface Sci.*, 2010, **350**, 110–116.
56 I. M. Modlin and G. Sachs, *Acid Related Diseases: Biology and Treatment*, 2004.
57 M. Solé, N. Rius and J. G. Lorén, *Int. Microbiol.*, 2000, **3**, 39–43.
58 B. J. Johnson, B. Lin, R. A. Rubin and A. P. Malanoski, *BMC Res. Notes*, 2009, **2**, 226.
59 M. Solé, A. Francia, N. Rius and J. G. Lorén, *Lett. Appl. Microbiol.*, 1997, **25**, 81–84.
60 D. J. Arp, P. S. G. Chain and M. G. Klotz, *Annu. Rev. Microbiol.*, 2007, **61**, 503–528.
61 K. A. Poelstra, N. A. Barekzi, A. M. Rediske, A. G. Felts, J. B. Slunt and D. W. Grainger, *J. Biomed. Mater. Res.*, 2002, **60**, 206–215.
62 X. He, Y. Kuang, Y. Li, H. Zhang, Y. Ma, W. Bai, Z. Zhang, Z. Wu, Y. Zhao and Z. Chai, *Nanotoxicology*, 2012, **6**, 233–240.

63 A. Thill, O. Zeyons, O. Spalla, F. Chauvat, J. Rose, M. Auffan and A.-M. Flank, *Environ. Sci. Technol.*, 2006, **40**, 6151–6156.
64 K. Li, Y. Chen, W. Zhang, Z. Pu, L. Jiang and Y. Chen, *Chem. Res. Toxicol.*, 2012, **25**, 1675–1681.
65 A. García, L. Delgado, J. A. Torà, E. Casals, E. González, V. Puntes, X. Font, J. Carrera and A. Sánchez, *J. Hazard. Mater.*, 2012, **199–200**, 64–72.
66 I. M. El-Nahhal, S. M. Zourab, F. S. Kodeh, M. Selmane, I. Genois and F. Babonneau, *Int. Nano Lett.*, 2012, **2**, 14.
67 F. Herzog, M. J. D. Clift, F. Piccapietra, R. Behra, O. Schmid, A. Petri-Fink and B. Rothen-Rutishauser, *Part. Fibre Toxicol.*, 2013, **10**, 1–14.
68 F. Herzog, K. Loza, S. Balog, M. J. D. Clift, M. Epple, P. Gehr, A. Petri-Fink and B. Rothen-Rutishauser, *Beilstein J. Nanotechnol.*, 2014, **5**, 1357–1370.
69 P. Demokritou, S. Gass, G. Pyrgiotakis, J. M. Cohen, W. Goldsmith, W. McKinney, D. Frazer, J. Ma, D. Schwegler-Berry, J. Brain and V. Castranova, *Nanotoxicology*, 2013, **7**, 1338–1350.

http://doc.rero.ch